Annual Methodological Archive Research Review
http://amresearchreview.com/index.php/Journal/about
Volume 4, Issue 1 (2026)

Online ISSN 3007-3197
Print ISSN 3007-3189

http://amresearchreview.com/index.php/Journal/about

Effect Of Calcination Temperature On The Microstructure And Physical Properties Of $Ba_{0.75-x}ca_xla_{0.30}fe_{12}co_{0.25}ti_{0.15}o_{19}$ M-Type Barium Hexaferrites

Muhammad Shahed Saqib
Faculty of Sciences, The Superior University Lahore, Pakistan
Email: shahidsaqib222@gmail.com

Fayyaz Ahmad
Faculty of Sciences, The Superior University Lahore, Pakistan
Email: fayyaz.ahmad.fsd@superior.edu.pk

ABSTRACT

$Ba_{0.75-x}$ $Ca_xLa_{0.3}0Fe_{12}Co_{0.25}Ti_{0.15}O_{19}$ M-type barium hexaferrite powders were synthesized by the solid-state reaction route and the powders were heat treated for 12 hours at four progressively higher temperatures (1130, 1140, 1150, and 1160 °C) to trace the effect of thermal treatment on phase formation, crystallite growth, surface morphology and magnetic behavior within this system. The X-ray diffraction pattern at all the calcination temperatures revealed a high percentage of one hexagonal M-type magneto plumbite phase corresponding to JCPDS card No. 43-0002 and weak traces of another α-Fe_2O_3 phase indicating the incomplete crystallization at the lower temperature end. The principal reflections were used to derive the crystallite size using the Debye–Scherrer relation, which showed that as the calcination temperature increased, the crystallite size increased progressively from 41.72 nm at 1130 °C to 89.75 nm at 1160 °C, in line with the expected thermally induced grain growth. Scanning electron microscopy showed monodisperse, hexagonal nanoplates consistent with the magnetoplumbite structure, which become coarser and more agglomerated as the temperature rises. Vibrating sample magnetometry revealed that saturation magnetization remained nearly constant between 1130 °C and 1140 °C (around 63.30 emu/g), then decreased to 57.43 emu/g at 1150 °C and further to 49.99 emu/g at 1160 °C. Meanwhile, coercivity increased from 2024 Oe to 2451 Oe over this temperature range. These patterns suggest a competition between grain growth, cation redistribution among the tetrahedral, octahedral and bipyramidal sites in the hexaferrite lattice and the resulting changes in super exchange interaction strength and magneto crystalline anisotropy. Overall, the findings demonstrate that calcination temperature is an effective and simple means to tune the crystallite size, remanence and coercivity of La–Ca–Co–Ti substituted M-type barium hexaferrites, useful in permanent magnets and high-frequency applications.

Keywords: Barium Hexaferrite; Calcination Temperature; X-Ray Diffraction; Scherrer Equation; Sem; Vibrating Sample Magnetometer; Coercivity; Saturation Magnetization.

Annual Methodological Archive Research Review
http://amresearchreview.com/index.php/Journal/about
Volume 4, Issue 1 (2026)

Online ISSN 3007-3197
Print ISSN 3007-3189

http://amresearchreview.com/index.php/Journal/about

INTRODUCTION

Historical Background and Technological Significance

The mineral magneto plumbite, which names this entire family of compounds, was first identified in 1925. It wasn't until 1938 that Adelsköld determined its actual structure: a hexagonal configuration with the nominal formula $PbFe_{12}O_{19}$ [1,2]. Barium hexaferrite only arrived in laboratories after World War II, when a Philips research team led by J. L. Snoek discovered that $BaFe_{12}O_{19}$ shares the same magnetoplumbite structure. They aimed to turn this discovery into a commercial product, which succeeded in 1952. Researchers Went, Ruthenium, Garter and van Oosterhout introduced “Ferroxidase,” the first permanent magnet made of hard ferrite. It had a coercive force near 240 kA/m a remanent induction of 0.20–0.21 T and a maximum energy product of around 6.8 kJ/m³. While modest by today's standards, this magnet was revolutionary at the time because it did not require cobalt, nickel or other strategic metals. [3].

After over seventy years, hard hexaferrites remain the most widespread type of permanent magnets today. This is largely due to their low material cost, high resistance to corrosion and demagnetization and the lack of eddy-current losses that affect metallic magnets, rather than their magnetic strength [4]. In its unsubstituted bulk single-crystal form, $BaFe_{12}O_{19}$ exhibits a saturation magnetization of approximately 72 emu/g, a Curie temperature close to 450 °C, and an impressive magneto-crystalline anisotropy field of about 17 kOe along the c-axis. These values are used as models for comparing all the variants, such as those that were substituted and nanostructured, including the variant studied in this paper [2]. The thermal stability and anisotropy in hard hexaferrites are essential to make this material competitive to the rare earth magnet for applications where the highest energy product is not a requirement.

Nanostructured Magnetic Materials and Ferrites

Reducing a magnetic material to the nanometer scale alters its behavior beyond bulk theory predictions: the surface-to-volume ratio increases significantly, domain configurations change and magnetic anisotropy depends on particle size [5,6]. This size-dependent behavior is a major reason why research on gas-phase, solution-based and solid-state methods for producing magnetic nanoparticles has been ongoing. These nanoparticles are used in data storage, biomedical labeling and microwave-absorbing coatings [7,8]. Among magnetic oxides, ferrites are notable for combining strong magnetization with high electrical resistance, chemical stability and low-cost materials [2,9]. This combination surpasses what metallic magnets can offer, as their high conductivity causes eddy-current losses that ferrites largely minimize. Ferrites are naturally divided into two categories based on how they react to an applied magnetic field [9]. Soft ferrites, including spinel (MFe_2O_4) and garnet structures, magnetize and demagnetize easily, producing narrow hysteresis loops with low coercivity. This property makes them ideal for use in transformer cores, inductors and high-frequency signal components [9,10]. Hard ferrites are characterized by wide hysteresis loops, high coercivity and a strong resistance to demagnetization after magnetization. These properties make them ideal for applications like permanent magnets, recording media and microwave absorbers or circulators [2,11]. Barium

Annual Methodological Archive Research Review
http://amresearchreview.com/index.php/Journal/about
Volume 4, Issue 1 (2026)

Online ISSN 3007-3197
Print ISSN 3007-3189
http://amresearchreview.com/index.php/Journal/about

hexaferrite ($BaFe_{12}O_{19}$) and its strontium counterpart ($SrFe_{12}O_{19}$) are the most well-known members of the hard hexagonal ferrite family, which is the focus of this work.

M-type Hexagonal Ferrites: Structure and Cation Substitution

M-type hexaferrites possess a hexagonal magnetoplumbite structure, classified under space group P63/mmc. In this structure, Fe^{3+} ions are arranged across five distinct crystallographic sites: three octahedral (2a, 4f2, 12k), one tetrahedral (4f1) and one trigonal bipyramidal (2b). The large divalent ion (Ba2+ or Sr2+) is found in the spaces between layers of oxygen atoms arranged in a hexagonal lattice [2,12]. It is a net moment of the unit cell that is due to an incomplete cancellation between antiparallel Fe3+ spin sublattices, which are coupled through Fe^{3+}–O_2–Fe^{3+} super exchange. Moreover, a prominent uniaxial anisotropy along the hexagonal c-axis, a key feature of this structure, is another property that makes this family stand out, in addition to the large coercivity [13,14].

Replacing Ba^{2+}/Sr^{2+} and Fe^{3+} sites with different cations has proven effective in tuning the structural and magnetic properties of M-type hexaferrites for specific uses. Substituting some Ba^{2+} or Sr^{2+} ions with smaller alkaline-earth or rare-earth ions like Ca^{2+} and La^{3+} refines the crystallite size and causes minor adjustments to the lattice parameters, all while maintaining the magnetoplumbite phase [15,16,17]. Pairing a transition-metal cation with a tetravalent ion on the Fe^{3+} sublattice, such as Co^{2+} and Ti^{4+}, is a common approach. It provides a charge-balanced method to modify saturation magnetization and coercivity in both Ba- and Sr-based hexaferrites[18,19]. La–Co co-substitution in strontium hexaferrite has also been demonstrated to modify the anisotropy field and domain structure without affecting the original hexagonal phase [20,21]. Work on Cd^{2+}- and Pb^{2+}-substituted systems has investigated how differences in ionic size affect phase purity and magnetic behavior in the M-type lattice [22,23].

The feasibility of these substitutions primarily depends on ionic size and charge balance. Ba2+ fits into its site with twelve-fold oxygen coordination, having an effective ionic radius of approximately 1.61 Å. This is comparable to Sr^{2+}'s 1.44 Å, Ca^{2+}'s about 1.34 Å in the same coordination and La^{3+}'s roughly 1.36 Å. Since La^{3+} is close enough in size to Ba^{2+}, limited substitution is structurally feasible. However, the size difference is sufficient to cause a measurable contraction of the lattice and a reduction in crystallite size as the substitution level increases [24]. Since La^{3+} has one more positive charge than Ba^{2+} it replaces, the substitution alone is not charge-neutral. To maintain overall charge balance, it is paired with an equal amount of Co^{2+} on the Fe^{3+} sublattice, which has one less positive charge than Fe^{3+}. This explains the widely recognized “La–Co” substitution scheme in M-type hexaferrites. [20]. Ca^{2+} is isovalent with Ba^{2+} and can substitute without needing charge compensation elsewhere. Meanwhile, the extra Co^{2+}–Ti^{4+} pair on the Fe^{3+} sites in the current composition is itself charge-balanced (with Co^{2+} + Ti^{4+} averaging +3, similar to two Fe^{3+} ions). This provides a second, independent way to control the Fe^{3+} sublattice occupancy, which influences the saturation magnetization and anisotropy [18,19]. The studied composition, $Ba_{0.75-x}Ca_xLa_{0.30}Fe_{12}Co_{0.25}Ti_{0.15}O_{19}$, incorporates both mechanisms simultaneously Ca^{2+} and La^{3+} substituting on the Ba^{2+} site and Co^{2+}–Ti^{4+} replacing Fe^{3+} within a single M-type hexaferrite.

Annual Methodological Archive Research Review
http://amresearchreview.com/index.php/Journal/about
Volume 4, Issue 1 (2026)

Online ISSN 3007-3197
Print ISSN 3007-3189
http://amresearchreview.com/index.php/Journal/about

Effect of Calcination Temperature and Research Objective

Because the magnetoplumbite phase requires a high-temperature solid-state reaction between oxide and carbonate precursors to form completely, calcination temperature is one of the most critical processing factors affecting phase purity, crystallite size and residual secondary-phase content in hexaferrite powders [25,26]. Insufficient heat results in unreacted α-Fe_2O_3 and other iron-oxide phases remaining; excessive heat, however, causes grain coarsening and can alter the proportion of single-domain and multi-domain particles, impacting both saturation magnetization and coercivity [27,28]. The establishment of this correlation of the temperature and the properties of the microstructure of a particular composition is necessary to optimize the conditions of synthesis and understand the magnetic behavior that is obtained [29]. In this study, $Ba_{0.75-x}Ca_xLa_{0.3}0Fe_{12}Co_{0.25}Ti_{0.15}O_{19}$ M-type hexaferrite powder are synthesized by solid-state reaction method. It evaluates the variation in phases, crystallite size, lattice structure (X-ray diffraction) and magnetic properties like saturation magnetization, remanence and coercivity (by vibrating sample magnetometry) over four different calcination temperatures (1130, 1140, 1150 and 1160 °C). The resulting structure–property correlations are supposed to assist in the selection of calcination conditions for the bahefs with substituted La–Ca–Co–Ti for the application of permanent magnets and high-frequency devices [2,18].

MATERIALS AND METHODS

Materials and Synthesis

$Ba_{0.75-x}Ca_xLa_{0.30}Fe_{12}Co_{0.25}Ti_{0.15}O_{19}$ hexaferrite powders were prepared using the conventional solid-state reaction method, a preferred approach for hexaferrite production due to its simplicity, scalability, and the absence of organic solvents [30,31]. High-purity precursors such as barium carbonate ($BaCO_3$), calcium carbonate ($CaCO_3$), lanthanum oxide (La_2O_3), iron(III) oxide (Fe_2O_3), cobalt(II) oxide (CoO) and titanium dioxide (TiO_2) were weighed according to the molar ratios required by the target composition's cation stoichiometry. During calcination, the carbonate precursors decompose, releasing CO_2, while the metal oxides interdiffusion and react in the solid state to form the hexagonal magnetoplumbite structure. Using oxide and carbonate precursors instead of nitrates or organometallic salts is standard in solid-state hexaferrite synthesis, as it prevents residual anions from causing secondary phases [32,33].

The precursor powders were mixed and ground mechanically using a pestle and mortar to achieve close contact between reactant particles, as solid-state diffusion is slow and the reaction rate depends heavily on how finely and uniformly the powders are dispersed. This also explains why solid-state synthesis, unlike solution-based methods such as sol-gel or co-precipitation, requires relatively high temperatures (usually 1000–1500 °C) to proceed efficiently: unlike wet-chemical approaches where reactants are pre-mixed at the atomic or molecular level in solution, solid-state reactants must diffuse across grain boundaries, a process that is slower and less complete unless driven by increased thermal energy [31,34]. Because of the reduced reaction temperature and more uniform and fine particles, wet-chemical methods such as co-precipitation, sol-gel combustion and hydrothermal routes have been used. But the extra cost and complexity of these methods is caused by the use of organic

Annual Methodological Archive Research Review
http://amresearchreview.com/index.php/Journal/about
Volume 4, Issue 1 (2026)

Online ISSN 3007-3197
Print ISSN 3007-3189
http://amresearchreview.com/index.php/Journal/about

precursors/surfactants and the potential for organic residues such as carbon or hydroxides which require subsequent burning off. The choice of the solid-state method was specifically made to isolate the effect of the calcination temperature, with a known precursor chemistry, eliminating the effects of wet-chemical processes. The precursor mixture was homogenized and then the batches were calcined in air for 12 hours at the following temperatures: 1130 °C, 1140 °C, 1150 °C and 1160 °C. In this way, the effect of calcination temperature could be studied separately, holding the other parameters of the process constant. The selected temperature range is similar to the range reported for solid-state reaction and complete crystallization of M-type hexagonal phase in Ba- and Sr-based hexaferrites [22,26]. After calcination, all batches were cooled down to room temperature in a furnace and then slowly ground to a fine powder for characterization.

Characterization Techniques

Powder X-ray diffraction (Cu-Kα radiation, $\lambda = 1.5406$ Å) was used to identify the phases and calculate the crystallite size, both scanned in the range of $2\theta = 10–80°$. The diffraction peaks were compared with the JCPDS reference pattern of M-type hexaferrite (Card No. 43-0002) and the average crystallite size for each sample was calculated using the Debye–Scherrer equation $D = k\lambda/(\beta \cos\theta)$, with $k = 0.9$ suitable for the hexagonal system [14,34,36]. The interplanar spacing (d) of each reflection was calculated with the help of Braggs law $n\lambda = 2d \sin\theta$, as it is done in hexaferrite structures in the conventional way [2]. The interplanar spacings of a hexagonal unit cell such as the M-type magneto plumbite structure are given by $1/d^2 = (4/3)\cdot(h^2+hk+k^2)/a^2 + l^2/c^2$, where h, k and l are the Miller indices. This was the conventional relation adopted for calculating the dimensions of the unit-cell from the indexed hexagonal diffraction data [2]. The Williamson–Hall method is another approach that allows the identification of crystallite size and lattice strain effects by the use of an x-ray diffractogram in which the $\beta\cos\theta$ is plotted against $\sin\theta$ for a series of reflections. This method was studied in addition to the single peak Scherrer analysis used in this work as the principal size estimation technique [37]. The particle morphology and microstructural evolution was analyzed by scanning electron microscopy. Secondary electrons, which have low energy, can only escape from a very shallow surface layer and are chiefly responsible for the creation of topographic contrast, which is useful for identifying individual grains and their shape. Higher-energy backscattered electrons, however, give some additional information about the composition from slightly deeper within the sample [38]. Micrographs were taken with a 5 μm scale bar at a magnification of 100,000x, which showed excellent resolution of the morphology of the platelets observed in the M-type hexaferrite grains [10]. The magnetic hysteresis of the materials was measured at room temperature in a field range of ±10,000 Oe following the design concept first introduced by Foner [40]. It is based on Faraday's law of electromagnetic induction which states that when a magnetized sample is vibrated at a fixed frequency in the vicinity of pickup coils, an oscillating electromotive force is generated. This force is proportional to the magnetic moment and it is possible to obtain direct measurements of saturation magnetization (Ms), and remanent magnetization (Mr) and coercivity (Hc) from the obtained M–H loop [11]. These three main parameters were used to

Annual Methodological Archive Research Review
http://amresearchreview.com/index.php/Journal/about
Volume 4, Issue 1 (2026)

Online ISSN 3007-3197
Print ISSN 3007-3189
http://amresearchreview.com/index.php/Journal/about

calculate the remanence ratio (or squareness) of each sample, which was used as a qualitative indicator of the distribution of domains in each sample. Proximity to unity usually meant a greater amount of single domain regions [13].

RESULTS AND DISCUSSION

Hexaferrite powders of the formula $Ba_{0.75-x}Ca_xLa_{0.30}Fe_{12}Co_{0.25}Ti_{0.15}O_{19}$ were prepared by calcining the samples at 1130, 1140, 1150 and 1160 °C, and their structural, morphological and magnetic properties were investigated by X-ray diffraction, scanning electron microscopy and vibrating sample magnetometry. The effect of calcination temperature on phase purity, crystallite size and particle morphology and magnetic hysteresis parameters [2,26] is analyzed in the following sections.

Structural Analysis by X-ray Diffraction (XRD)

The well-known powder X-ray diffraction is still the preferred technique for the identification of crystalline phases, the lattice parameters and the crystallite size of polymer crystalline ceramics [34]. A diffraction pattern was obtained for all four calcined samples in the range of 2θ = 10–80°. The crystallite size (D) of each was then estimated using the FWHM (β) of its peaks, according to the Debye–Scherrer equation [14,36]:

$$D = k\lambda / (\beta \cos \theta)$$

where k is the Scherrer shape constant (0.9 for cubic and hexagonal systems), λ represents the wavelength of the incident Cu-Kα radiation (1.5406 Å) and θ is the Bragg angle for each reflection. The interplanar spacing (d) for each peak is derived using Bragg's law: $n\lambda = 2d \sin\theta$ [2].

XRD Patterns at 1130–1160 °C

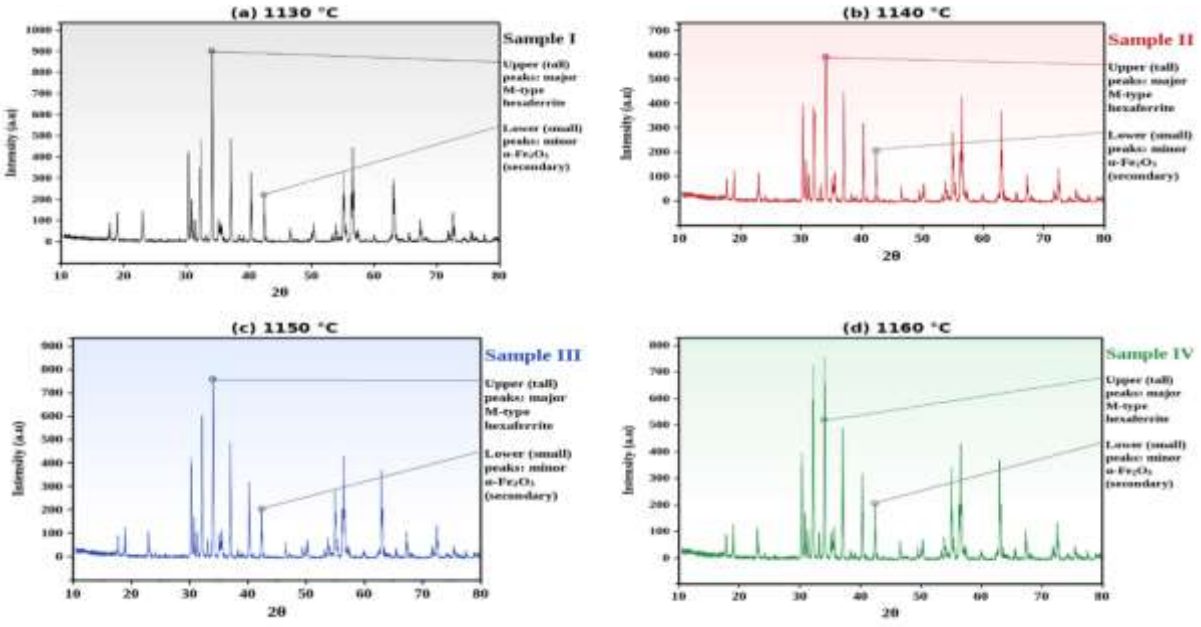


Figure 1. XRD patterns of the $Ba_{0.75-x}Ca_xLa_{0.30}Fe_{12}Co_{0.25}Ti_{0.15}O_{19}$ hexaferrite

Annual Methodological Archive Research Review
http://amresearchreview.com/index.php/Journal/about
Volume 4, Issue 1 (2026)

Online ISSN 3007-3197
Print ISSN 3007-3189

http://amresearchreview.com/index.php/Journal/about

calcined at (a) 1130 °C, (b) 1140 °C, (c) 1150 °C and (d) 1160 °C.

The XRD pattern can be used to tell a material's crystal structure apart; the angle of the scan is plotted on the horizontal axis, and each peak is a particular set of atomic planes reflecting X-rays at certain angles. The peaks in (a)–(d) of the figure are at the same angles, which means that all the samples are of the same crystal phase. The peaks become taller and narrower, however, when the calcination temperature is raised from 1130 °C to 1160 °C. A high peak is generally correlated with a larger and crystals graphically more perfect crystal in an XRD plot. Thus, from the visual observation it can be inferred from figure 1 that, with increase in calcination temperature, the size of the hexaferrite particles becomes larger and the structure becomes better.

Table 1. The parameters of structure obtained from the XRD pattern at the temperature 1130 °C (average crystallite size 41.72 nm).

2θ (deg.)	FWHM (deg.)	d-spacing (nm)	Crystallite Size (nm)
17.82	4.474	0.39	22.39
17.82	3.23137	0.44	19.81
19.03	3.00003	0.1212	71.47
23	2.88189	0.1047	81.49
30.3	2.79302	0.0859	98.82
32.39	2.52219	0.34	24.86
34.06	2.06889	0.0877	95.54
37.16	1.57966	0.0935	88.74
40.35	2.28894	0.36	22.9
42.35	2.04038	0.09	86.85
55.67	2.52219	0.1447	52.05
63.13	2.06889	0.2924	24.44

The pattern at 1130 °C (Figure 1a, Table 1) exhibits strong and well-resolved peaks, which are in good agreement with the positions in JCPDS Card No. 43-0002 for the M-type hexagonal magneto plumbite structure [2,12]. The narrow peaks and low background suggests that the sample was relatively crystalline even at the lowest calcination temperature. The presence of some low-intensity reflections compatible with the residual α-Fe2O3, however, indicate that the hexaferrite phase is still in the process of formation [25,33]. Average crystallite size calculated by Scherrer equation from the twelve most intense reflections varied from 19.8nm to 98.8nm with an average of 41.72nm for the entire sample.

Annual Methodological Archive Research Review
http://amresearchreview.com/index.php/Journal/about
Volume 4, Issue 1 (2026)

Online ISSN 3007-3197
Print ISSN 3007-3189

http://amresearchreview.com/index.php/Journal/about

Table 2. The structural parameters calculated from the XRD pattern at 1140 °C are average crystallite size = 53.02 nm.

2θ (deg.)	FWHM (deg.)	d-spacing (nm)	Crystallite Size (nm)
17.82	4.474	0.39	22.39
19.03	3.23137	0.44	19.81
22.89	3.00003	0.1212	71.48
30.3	2.88189	0.1047	81.49
32.18	2.79302	0.0859	98.87
34.06	2.52219	0.34	24.86
37.16	2.06889	0.0877	95.54
40.24	1.57966	0.0935	88.77
42.46	2.28894	0.36	22.89
55.05	2.04038	0.09	87.1
56.71	2.52219	0.1447	53.76
63.01	2.06889	0.2924	25.77

The single hexagonal phase remains at 1140 °C (Figure 1b, Table 2), where the main reflections become more intense than at 1130 °C, suggesting that the long-range crystalline order is improved. The peak positions are also very similar to those of JCPDS 43-0002 and indicate that the structure of magneto plumbite is not changed by the substitutions of La3+, Ca2+, Co2+ and Ti4+ [15,20]. However, the average crystallite size increases to 53.02 nm, which is 27% larger compared to the crystallite size measured at 1130 °C, suggesting that grain coarsening in the heat treated sample has begun.

Table 3. The average crystallite size from the XRD pattern at 1150 °C = 72.83 nm.

2θ (deg.)	FWHM (deg.)	d-spacing (nm)	Crystallite Size (nm)
17.82	4.474	0.39	22.39
18.03	2.28894	0.44	19.84
23	2.04038	0.1212	71.47
30.3	2.52219	0.54	15.8
32.18	2.79302	0.0859	98.87
34.06	2.52219	0.023	367.48
37.16	2.06889	0.0877	95.54
40.24	1.57966	0.0935	88.77

Annual Methodological Archive Research Review
http://amresearchreview.com/index.php/Journal/about
Volume 4, Issue 1 (2026)

Online ISSN 3007-3197
Print ISSN 3007-3189

http://amresearchreview.com/index.php/Journal/about

2θ (deg.)	FWHM (deg.)	d-spacing (nm)	Crystallite Size (nm)
42.46	2.28894	0.36	22.89
54	2.04038	0.09	87.51
56.71	2.52219	0.1447	53.76
63.01	2.06889	0.2924	25.77

The diffraction peaks are at this time much sharper and more intense, especially the high number of peaks between 2θ = 30–38° which corresponds to significant grain growth [28] (see Figure 1c, Table 3). The average crystallite size rises significantly to 72.83 nm, which is higher than that at 1140 °C, which indicates the presence of residual α-Fe2O3, albeit in low amounts. The residual secondary phase diminishes as the thermal treatment intensifies [25,27].

Table 4. Structural parameters obtained from the XRD pattern at 1160 °C (average crystallite size = 89.75 nm).

2Θ (DEG.)	FWHM (DEG.)	D-SPACING (NM)	CRYSTALLITE SIZE (NM)
17.82	4.474	0.39	22.39
20.17	3.23137	0.044	198.14
22.89	3.00003	0.1212	71.48
30.3	2.88189	0.1047	81.49
32.95	2.79302	0.0859	98.87
34.06	2.52219	0.34	24.86
37.95	2.06889	0.0877	95.54
40.24	1.57966	0.0935	88.77
42.46	2.28894	0.036	228.88
56.05	2.04038	0.09	87.1
56.71	2.52219	0.1447	53.76
63.43	2.06889	0.2924	25.77

The pattern from the highest tested calcination temperature, 1160 °C (Figure 1d, Table 4), clearly corresponds to JCPDS 43-0002, showing well-resolved, high-intensity reflections [2]. The average crystallite size reaches a peak of 89.75 nm, indicating ongoing diffusion-controlled grain growth established at lower temperatures [19,26]. Overall, Figure 1 indicates that all four samples maintain their pure, single-phase hexagonal magnetoplumbite structure throughout this temperature range. Additionally, increasing the calcination temperature from 1130 to 1160 °C

Annual Methodological Archive Research Review
http://amresearchreview.com/index.php/Journal/about
Volume 4, Issue 1 (2026)

Online ISSN 3007-3197
Print ISSN 3007-3189
http://amresearchreview.com/index.php/Journal/about

progressively sharpens and strengthens the M-type reflections in comparison to the minor α-Fe2O3 peaks [27].

Comparative XRD Analysis and Crystallite Size Trend

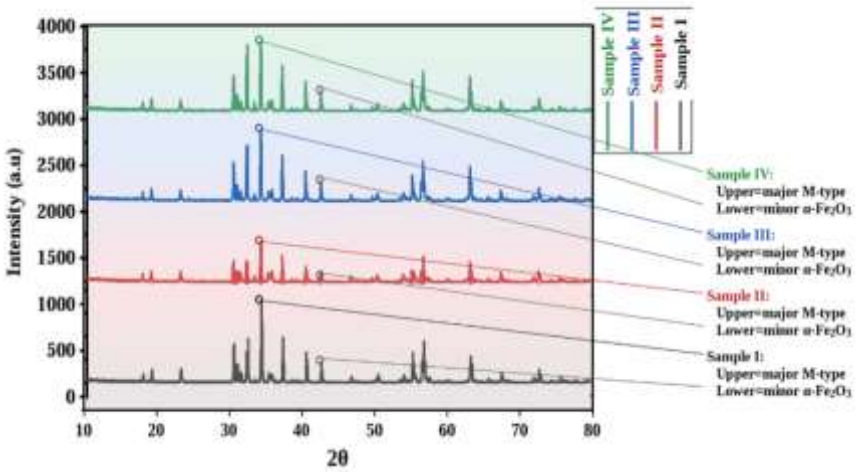


Figure 2. Stacked XRD patterns of the $Ba_{0.75-x}Ca_xLa_{0.30}Fe_{12}Co_{0.25}Ti_{0.15}O_{19}$ hexaferrite calcined at 1130, 1140, 1150 and 1160 °C.

Table 5. Variation of average crystallite size with calcination temperature.

Sample	Calcination Temperature (°C)	Average Crystallite Size (nm)
1	1130	41.72
2	1140	53.02
3	1150	72.83
4	1160	89.75

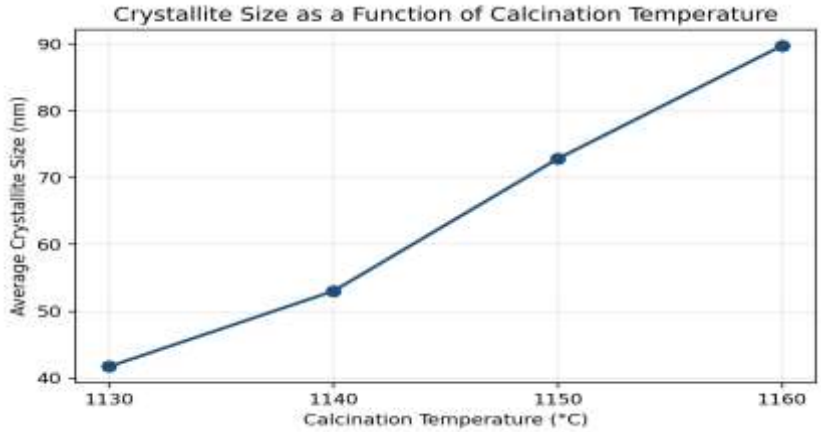


Figure 3. *Average crystallite size of $Ba_{0.75-x}Ca_xLa_{0.30}Fe_{12}Co_{0.25}Ti_{0.15}O_{19}$ as a function of calcination temperature (data of Table 5).*

Annual Methodological Archive Research Review
http://amresearchreview.com/index.php/Journal/about
Volume 4, Issue 1 (2026)

Online ISSN 3007-3197
Print ISSN 3007-3189

http://amresearchreview.com/index.php/Journal/about

Figure 3 aggregates all twelve peak measurements from each sample into a single average crystallite size value, plotted against calcination temperature. The graph shows a steady increase from left to right, no dips or plateaus, which means that there is a clear direct relationship between the two variables, with an increase in the calcination temperature increasing the crystallite size, with no opposing effect. The crystallite size of this hexaferrite increases by more than double (41.72 nm to 89.75 nm) with a rise in the calcination temperature from 370 °C to 400 °C, highlighting the high sensitivity of the crystallite size of this hexaferrite to calcination temperature. The main conclusion of the structure obtained from the stacked patterns in Figure 2 and the data in Table 5 and Figure 3, is that a steady and significant increase in crystallite size occurs with increasing calcination temperature, more than doubling in the temperature range 1130–1160 °C [14,25]. This is similar with other types of M-type hexaferrite, in which the process of calcination at temperature higher than about 1140 °C provides sufficient thermal energy to drive the solid state reaction and promote the diffusion-driven grain growth process, thus decreasing the amount of residual α-Fe2O3 [26,28]. Reflections of magnetoplumbite are found at nearly the same two theta values for all four samples, which means that the addition of La3+, Co2+ and Ca2+ to the Ba sublattice has little effect on the hexagonal unit cell as observed earlier for La–Co co-substituted M-type hexaferrites [17,19,20].

Surface Morphology by Scanning Electron Microscopy (SEM)

The morphology and the microstructural changes in the calcined powders were investigated by scanning electron microscopy [38]. Micrographs obtained at 100,000× magnification and a 5 μm scale bar for samples calcined at 1130 °C and 1140 °C, respectively.

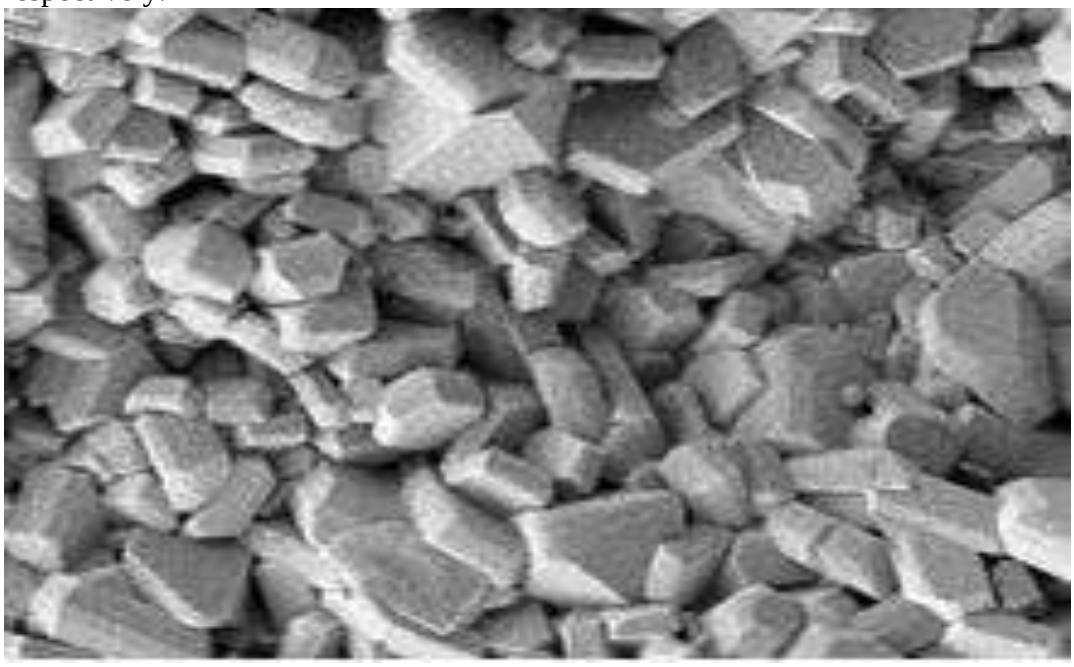


Figure 4. SEM micrograph of $Ba_{0.75-x}Ca_xLa_{0.3}0Fe_{12}Co_{0.25}Ti_{0.15}O_{19}$ calcined at 1130 °C (100,000×, 5 μm scale bar)

Annual Methodological Archive Research Review
http://amresearchreview.com/index.php/Journal/about
Volume 4, Issue 1 (2026)

Online ISSN 3007-3197
Print ISSN 3007-3189

http://amresearchreview.com/index.php/Journal/about

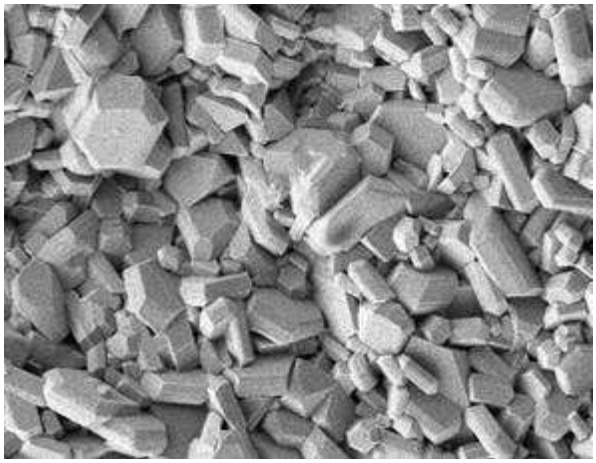


Figure 5. SEM micrograph of $Ba_{0.75-x}$ $Ca_xLa_{0.3}0Fe_{12}Co_{0.25}Ti_{0.15}O_{19}$ calcined at 1140 °C (100,000×, 5 µm scale bar).

In both micrographs, small, flat, angular pieces (chips) are seen and appear to be closely packed together in the fractured surface of a thin layer of glass. The angular, plate-like shape is a visual clue that the grains are likely to exhibit hexagonal magnetoplumbite structure confirmed by XRD; if the grains were round or fiber-like, this would indicate a different structure. The main difference between the images is the agglomeration and size of the chips in Figure 5 (1140 °C) compared to Figure 4 (1130 °C) which would be like a pile of chips being briefly heated so that adjacent pieces start to weld together at the edge of their contact. The grain growth and partial sintering observed in Table 5 is well supported by this slight temperature increase. The micrographs reveal a uniform and densely packed arrangement of hexagonal M-type magnetoplumbite grains, which is typical for these materials as confirmed by XRD [10,39]. The grains are in irregular outlines but always retain a platelet shape, and edges have faceted outlines like crystals which nucleate and grow mainly along the c-axis [2]. The 1140 °C powder has more irregular platelets than the 1130 °C powder, and some platelets are slightly fused together at the edges. This matches the increased crystallite size seen in XRD (see Table 5) and indicates that higher thermal energy promotes both crystallite growth within particles and neck formation between particles [26,28]. Neither micrograph shows a distinct second phase or different morphology, supporting the XRD conclusion that both samples remain nearly single-phase within this temperature range [27].

Magnetic Properties by Vibrating Sample Magnetometry (VSM)

The magnetic hysteresis (M–H) behavior of the calcined powders at room temperature was recorded using a vibrating sample magnetometer within an applied field range of ±10,000 Oe [40]. Saturation magnetization (Ms), remanent magnetization (Mr), and coercive field (Hc) were measured from each loop and are listed below for each calcination temperature.

Annual Methodological Archive Research Review
http://amresearchreview.com/index.php/Journal/about
Volume 4, Issue 1 (2026)

Online ISSN 3007-3197
Print ISSN 3007-3189

http://amresearchreview.com/index.php/Journal/about

M–H Loops at 1130–1160 °C

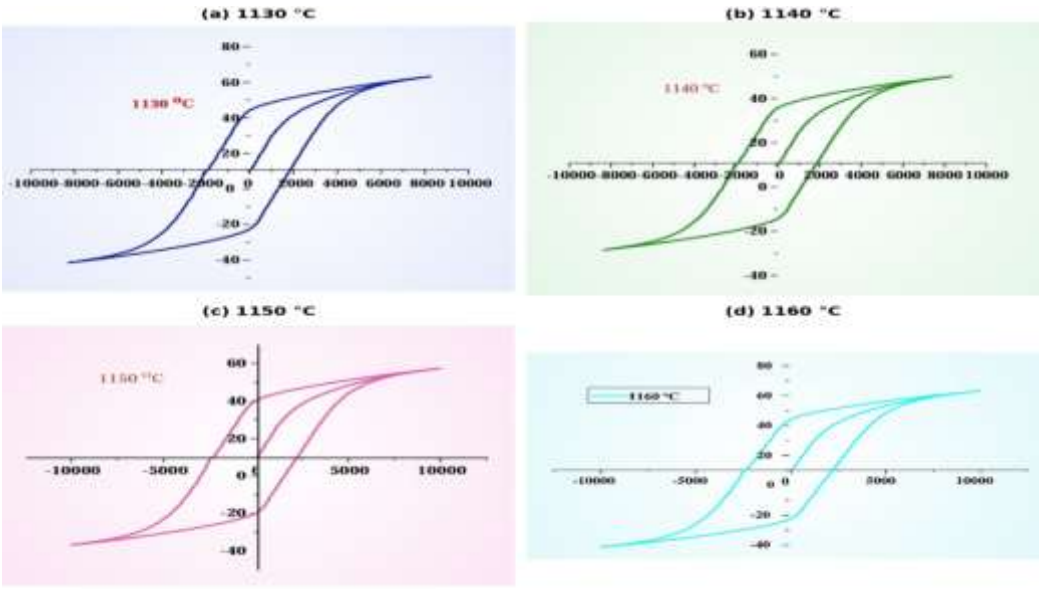


Figure 6. *Room-temperature M–H hysteresis loops of the* $Ba_{0.75-x}Ca_xLa_{0.30}Fe_{12}Co_{0.25}Ti_{0.15}O_{19}$ *hexaferrite calcined at (a) 1130 °C, (b) 1140 °C, (c) 1150 °C and (d) 1160 °C.*

Each panel in Figure 6 shows a hysteresis loop, where the magnetic field is swept from strongly negative to strongly positive along the horizontal axis, and the resulting magnetization of the sample is plotted on the vertical axis. The entire physical story can be understood from three key features of this S-shaped loop, all of which are easily observed in the figure.

First the maximum ‘altitude' of the curve before the curve levels off is the saturation magnetisation, which is the strongest magnetic response of the material.. Second, the distance between the two branches at zero applied field reflects the remanent magnetization or the remaining magnetism once the field is removed. Third and most visually obvious, is the loop's horizontal stretch before each branch crosses zero magnetization, which is the coercivity a direct visual indicator of how difficult it is to demagnetize the sample. Comparing panels (a) through (d), the loops gradually become shorter, indicating lower saturation magnetization, but wider, meaning higher coercivity, as the calcination temperature increases. This trend aligns precisely with the numerical data presented in Tables 6–9.

Table 6. *Magnetic parameters extracted from the M–H loop at 1130 °C.*

Parameter	Value
Saturation Magnetization (Ms)	63.31 emu/g
Remanent Magnetization (Mr)	43.27 emu/g

Annual Methodological Archive Research Review
http://amresearchreview.com/index.php/Journal/about
Volume 4, Issue 1 (2026)

Online ISSN 3007-3197
Print ISSN 3007-3189

http://amresearchreview.com/index.php/Journal/about

Parameter	Value
Coercivity (Hc)	2024 Oe

Table 7. *Magnetic parameters extracted from the M–H loop at 1140 °C.*

Parameter	Value
Saturation Magnetization (Ms)	63.30 emu/g
Remanent Magnetization (Mr)	35.06 emu/g
Coercivity (Hc)	2064 Oe

Table 8. *Magnetic parameters extracted from the M–H loop at 1150 °C.*

Parameter	Value
Saturation Magnetization (Ms)	57.43 emu/g
Remanent Magnetization (Mr)	39.49 emu/g
Coercivity (Hc)	2311 Oe

Table 9. *Magnetic parameters extracted from the M–H loop at 1160 °C.*

Parameter	Value
Saturation Magnetization (Ms)	49.99 emu/g
Remanent Magnetization (Mr)	43.43 emu/g
Coercivity (Hc)	2451 Oe

At 1130 °C, the sample exhibits a clear ferrimagnetic hysteresis loop with a saturation magnetization of 63.31 emu/g, remanent magnetization of 43.27 emu/g and coercivity of 2024 Oe (see Table 6). This combination of high Ms and Hc is characteristic of a hard-magnetic M-type hexaferrite, with a fine crystallite size of 41.72 nm (refer to Table 1). The small crystal size, close to the single-domain limit, enhances high coercivity by promoting domain-wall pinning at grain boundaries [13,14]. At 1140 °C, the saturation magnetization (63.30 emu/g, Table 7) remains largely unchanged from its value at 1130 °C, indicating that the Fe^{3+}–Fe^{3+} superexchange interactions across the tetrahedral, octahedral and bipyramidal sublattices are still largely intact [5]. The remanent magnetization decreases significantly to 35.06 emu/g, reducing the loop's squareness ratio (Mr/Ms), while coercivity slightly increases to 2064 Oe, corresponding with the observed crystallite coarsening seen in XRD [11].
Saturation magnetization decreases more distinctly to 57.43 emu/g at 1150 °C, with

Annual Methodological Archive Research Review
http://amresearchreview.com/index.php/Journal/about
Volume 4, Issue 1 (2026)

Online ISSN 3007-3197
Print ISSN 3007-3189
http://amresearchreview.com/index.php/Journal/about

coercivity continuing to increase to 2311 Oe (see Table 8). This reduction in Ms probably results from two combined factors: significant crystallite growth (72.83 nm, as shown in Table 3), which increases the proportion of the sample in a multi-domain state and a possible redistribution of cations among the five inequivalent Fe^{3+} sites in the M-type structure, which can weaken the overall superexchange interactions [19,20]. The 1160 °C sample shows the lowest saturation magnetization in the series at 49.99 emu/g, but it has the highest coercivity at 2451 Oe and a remanence of 43.43 emu/g (Table 9). The significant drop in Ms is due to the large crystallite size of 89.75 nm (Table 4) at this temperature, which causes more grains to switch from single-domain to multi-domain states. This transition decreases the overall magnetization, although coercivity is still affected by anisotropy and domain-wall pinning at residual grain-boundary defects [18,22].

Comparative Magnetic Analysis

retantivity reaches to 43.43 emu/g. While coercivity reaches to a value of 2451 Oe

4.3.5 Magnetic Hysteresis Loop for all samples

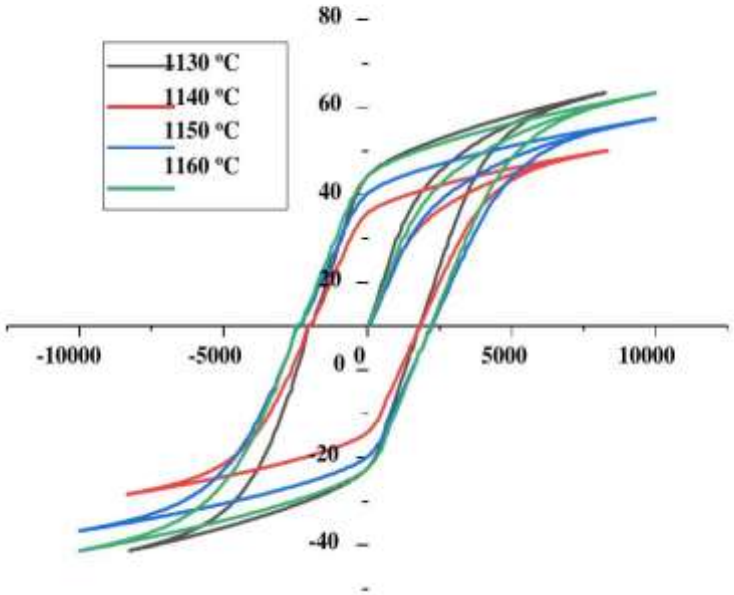


Figure 7. *Overlay of MH hysteresis loops of the hexaferrite* $Ba_{0.75-x}Ca_xLa_{0.3}0Fe_{12}Co_{0.25}Ti_{0.15}O_{19}$ *calcined at 1130–1160 °C.*

As the four loops in Figure 7 have the same axes, it is evident that, without resorting to any tabulated values, the relationship between the strength of the magnetisation and the coercivity of the four is not the same. The innermost and narrowest loop (1130 °C) is the lowest vertically but crosses the horizontal axis at a lower location. The outermost and widest loop is the 1160 °C loop, which doesn't go as high, but extends further along the horizontal axis before crossing the zero line. Taller loops are narrower and shorter loops are wider and show generally a balance in the visual appearance between saturation magnetization and coercivity in the calcination series.

Annual Methodological Archive Research Review
http://amresearchreview.com/index.php/Journal/about
Volume 4, Issue 1 (2026)

Online ISSN 3007-3197
Print ISSN 3007-3189

http://amresearchreview.com/index.php/Journal/about

Table 10. *Magnetic parameters (Ms, Mr and Hc) as a function of calcination temperature.*

Calcination Temperature (°C)	Ms (emu/g)	Mr (emu/g)	Hc (Oe)
1130	63.31	43.27	2024
1140	63.30	35.06	2064
1150	57.43	39.49	2311
1160	49.99	43.43	2451

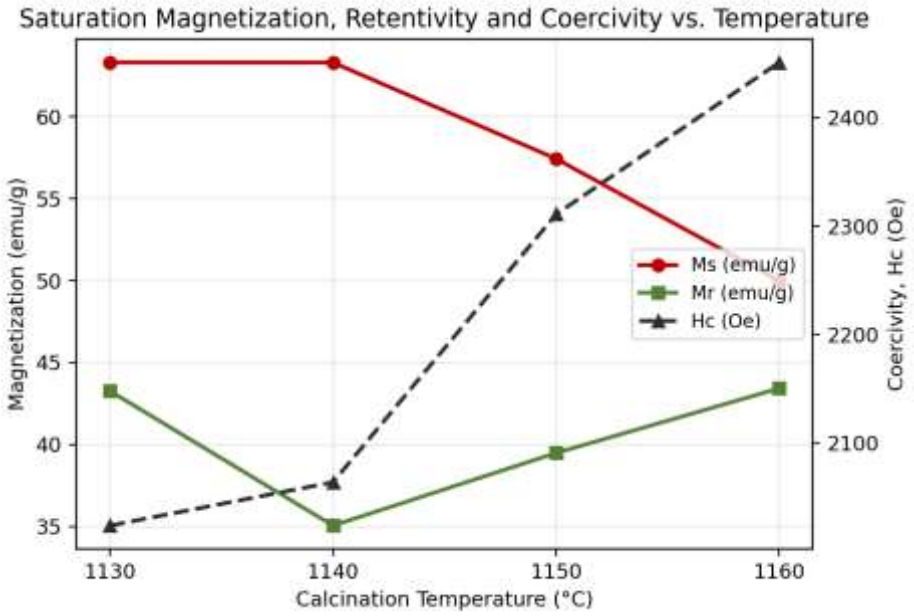


Figure 8. *Variation of saturation magnetization (Ms), remanent magnetization (Mr) and coercivity (Hc) with calcination temperature (data of Table 10).*

The trends of all three magnetic parameters are compared side by side in Figure 8 which shows all three parameters in the same graph. The saturation magnetization and coercivity curves move in opposite directions as temperature increases one decreases while the other increases crossing over at some point during the series. This crossing is a visual confirmation of the inverse effect of factors that favour crystallite growth at higher calcination temperatures, which reduces the magnetization, but enhances the coercivity as discussed in this section. The situation is different for the remanent magnetization curve, which first decreases, and then increases again to form a shallow U-shape, which means that not all magnetic parameters behave in the same straightforward way as a function of calcination temperature [28]. The coercivity has increased consistently from 2024 Oe @ 1130 °C to 2451 Oe @ 1160 °C or about 21% increase [13]. The remanent magnetization, however, does not follow the pattern, decreasing to a minimum of 35.06 emu/g at 1140 °C, and then increasing to 43.43 emu/g at 1160 °C, close to the value at 1130 °C.

These trends align well with both the crystallite-size changes observed in XRD

Annual Methodological Archive Research Review
http://amresearchreview.com/index.php/Journal/about
Volume 4, Issue 1 (2026)

Online ISSN 3007-3197
Print ISSN 3007-3189
http://amresearchreview.com/index.php/Journal/about

(Section 3.1) and the coarsening seen through SEM (Section 3.2): as the calcination temperature increases, grain growth shifts the microstructure away from the single-domain state that supports high saturation magnetization. Simultaneously, it enhances lattice perfection and introduces grain-boundary pinning sites, resulting in higher coercivity [5,6]. The saturation magnetization of this ferrimagnet, such as hexaferrite, is primarily determined by the strength of Fe^{3+}–O^{2-}–Fe^{3+} superexchange interactions across the 2a, 2b, 4f1, 4f2, and 12k sublattices [2,13]; Any temperature-dependent redistribution of Ca^{2+}, La^{3+}, Co^{2+} and Ti^{4+} among these sites, combined with microstructural coarsening, would likely further influence the net moment as observed [18,20]. The increasing coercivity, despite the decrease in Ms, indicates that magnetocrystalline anisotropy and microstructural pinning are the primary mechanisms controlling coercivity in this system, rather than solely single-domain particle-size effects [14,19].

Correlation Between Structural and Magnetic Properties

Analyzing the XRD and VSM results together shows that as the average crystallite size decreases, the saturation magnetization increases across the calcination series. Conversely, larger crystallite sizes correspond to higher coercivity [25,26]. As the crystallite size increases from 41.72 nm to 89.75 nm, Ms decreases from about 63 emu/g to 50 emu/g, while Hc increases from 2024 Oe to 2451 Oe. This common behaviour of the sub-100nm hard hexagonal ferrite magnetic grains illustrates that the effective magnetic moment per unit mass of the magnetic material decreases when the grain size increases and a transition from nearly single domain to a combination of both single and multi domain grains occurs. However, these improvements in structural quality and magnetocrystalline anisotropy field do not diminish the coercivity, but can, in fact, increase it [6,13,14]. From a practical point of view, the results of these studies suggest that the lower temperature range of 1130-1140 °C will yield a powder with a high Ms and moderate Hc values, suited for applications with high magnetization requirements. However, when the calcination temperature is in the upper end of the range (1150-1160 °C), the resulting powder has a lower Ms and higher Hc suitable for use in permanent-magnets manufacturing where coercivity is important [2,18,19].

SUMMARY

The $Ba_{0.75-x}$ $Ca_xLa_{0.3}0Fe_{12}Co_{0.25}Ti_{0.15}O_{19}$ M-type hexaferrite powders were synthesized by solid-state reaction [30] and subsequently calcinated at different temperatures (1130, 1140, 1150 and 1160 °C) to investigate the effect of calcination temperature on the structural, morphological and magnetic properties of the powders. At all four temperatures x-ray diffraction showed a predominately single phase hexagonal magnetoplumbite structure (JCPDS Card No. 43-0002) with minor α-Fe_2O_3 impurities which decreased in intensity as the calcination temperature was increased . The crystallite size calculated by Debye–Scherrer equation was found to increase systematically from 41.72 nm to 89.75 nm in each sample, which shows the grain growth in the series due to thermal activation. This was confirmed by scanning electron microscopy, which showed monodisperse hexagonal nanoplates that were darker and more aggregated with increasing calcination temperature. The saturation

Online ISSN 3007-3197
Print ISSN 3007-3189

magnetization was found to drop from 63.31 emu/g at 1130 °C to 49.99 emu/g at 1160 °C from the vibrating sample magnetometry results. Coercivity rose from 2024 Oe to 2451 Oe during this time period. Overall, the results showed that the processing parameter of calcination temperature is an effective and readily adjustable parameter to control crystallite size, remanence and coercivity of La–Ca–Co–Ti substituted M-type barium hexaferrites. The temperature ranges from 1130 to 1140 °C is the range for permanent magnet applications and high frequency applications due to the enhanced magnetization properties in this range, respectively.

References

[1] Adelsköld, V. (1938). X-ray studies on magneto-plumbite, PbO·6Fe2O3, and other substances resembling "beta-alumina," Na2O·11Al2O3. Arkiv för Kemi, Mineralogi och Geologi, 12A(29), 1–9.

[2] Pullar, R. C. (2012). Hexagonal ferrites: A review of the synthesis, properties and applications of hexaferrite ceramics. Progress in Materials Science, 57(7), 1191–1334.

[3] Went, J. J., Rathenau, G. W., Gorter, E. W., & van Oosterhout, G. W. (1952). Ferroxdure, a class of new permanent magnet materials. Philips Technical Review, 13, 194–208.

[4] de Julián Fernández, C., Sangregorio, C., de la Figuera, J., Belec, B., Makovec, D., & Quesada, A. (2021). Progress and prospects of hard hexaferrites for permanent magnet applications. Journal of Physics D: Applied Physics, 54, 153001.

[5] Roduner, E. (2006). Size matters: why nanomaterials are different. Chemical Society Reviews, 35(7), 583–592.

[6] Peddis, D., Cannas, C., Musinu, A., & Piccaluga, G. (2009). Magnetism in nanoparticles: beyond the effect of particle size. Chemistry – A European Journal, 15(32), 7822–7829.

[7] Kruis, F. E., Fissan, H., & Peled, A. (2012). Synthesis of nanoparticles in the gas phase for electronic, optical and magnetic applications – a review. Journal of Aerosol Science, 29(5), 511–535.

[8] Lead, J. R., & Wilkinson, K. J. (2006). Aquatic colloids and nanoparticles: current knowledge and future trends. Environmental Chemistry, 3(3), 159–171.

[9] Smit, J., & Wijn, H. P. J. (1959). Ferrites: Physical properties of ferrimagnetic oxides in relation to their technical applications. Eindhoven, The Netherlands: Philips Technical Library.

[10] Ita, B., & Murugavel, P. (2003). Magnetic properties of lanthanum orthoferrite fine powders prepared by different chemical routes. Journal of Chemical Sciences, 115(5), 519–524.

[11] Petcharoen, K., & Sirivat, A. (2012). Synthesis and characterization of magnetite nanoparticles via chemical co-precipitation method. Materials Science and Engineering: B, 177(5), 421–427.

[12] Shepherd, P., Mallick, K., & Green, R. J. (2007). Magnetic and structural properties of M-type barium hexaferrite prepared by co-precipitation. Journal of Magnetism and Magnetic Materials, 311(2), 683–692.

Annual Methodological Archive Research Review
http://amresearchreview.com/index.php/Journal/about
Volume 4, Issue 1 (2026)

Online ISSN 3007-3197
Print ISSN 3007-3189

http://amresearchreview.com/index.php/Journal/about

[13] Jones, G., & Parker, S. (2016). Domain structure of the single crystal hexagonal ferrite. IEEE Transactions on Magnetics, 26(5), 2804–2806.

[14] Sözeri, H. (2009). Simple recipe to synthesize single-domain BaFe12O19 with high saturation magnetization. Journal of Magnetism and Magnetic Materials, 321(18), 2717–2722.

[15] Iqbal, M. J., & Ashiq, M. N. (2010). Physical, electrical and dielectric properties of calcium substituted strontium hexaferrite SrFe12O19 nanoparticles synthesized by co-precipitation method. Journal of Magnetism and Magnetic Materials, 322(13), 1720–1726.

[16] Singh, V. P., Kumar, G., Kumar, A., Rai, R. S., Valente, M. A., Batoo, K. M., & Singh, M. (2016). Structural, magnetic and Mössbauer study of BaLaxFe12−xO19 nanohexaferrites synthesized via sol-gel auto-combustion technique. Ceramics International, 42(4), 5011–5017.

[17] Ashiq, M. N., Qureshi, R. B., Malana, M. A., & Ehsan, M. (2015). Fabrication, structural, dielectric and magnetic properties of tantalum and potassium doped M-type strontium calcium hexaferrites. Journal of Alloys and Compounds, 651, 266–272.

[18] Dong, C., & Wang, X. (2014). Microwave magnetic and absorption properties of M-type ferrite BaCoxTixFe12−2xO19 in the Ka band. Journal of Magnetism and Magnetic Materials, 354, 340–344.

[19] Rehman, K. M. U., & Liu, X. (2017). Synthesis of Sr0.7YxLa0.3−xFe12−yCoyO19 hexaferrites: structural and magnetic properties prepared by the solid-state reaction method. Chinese Journal of Physics, 55(5), 1780–1786.

[20] Kikuchi, T., Nakamura, T., Yamasaki, T., Nakanishi, M., Fujii, T., Takada, J., & Ikeda, Y. (2010). Magnetic properties of the La–Co substituted M-type strontium hexaferrites prepared by the polymerizable complex method. Journal of Magnetism and Magnetic Materials, 322(16), 2381–2385.

[21] Junliang, L., & Wei, Z. (2009). Synthesis and magnetic properties of quasi-single domain M-type barium hexaferrite powders via sol-gel auto-combustion: Effects of pH and the ratio of citric acid to metal ions. Journal of Alloys and Compounds, 479(1), 863–869.

[22] Din, M. F., & Ahmad, I. (2014). Influence of Cd substitution on structural, electrical and magnetic properties of M-type barium hexaferrites co-precipitated nanomaterials. Journal of Alloys and Compounds, 584, 646–651.

[23] Hussain, & Maqsood, A. (2008). Structural and electrical properties of Pb-doped Sr-hexaferrites. Journal of Alloys and Compounds, 466(1), 293–298.

[24] Shannon, R. D. (1976). Revised effective ionic radii and systematic studies of interatomic distances in halides and chalcogenides. Acta Crystallographica Section A, 32(5), 751–767.

[25] Ataie, A., & Zojaji, S. (2007). Synthesis of barium hexaferrite nano-particles via mechano-combustion route. Journal of Alloys and Compounds, 431(2), 331–336.

[26] Mohammed, J., Batoo, K. M., Mukhtar, G., Labis, J. P., Raslan, E. H., Hadi, M., & Srivastava, A. K. (2022). Crystal-structure analysis, Raman spectroscopy, dielectric measurements, magnetic and optical properties of Cr3+–Ni2+-

Online ISSN 3007-3197
Print ISSN 3007-3189

substituted Co2Y-type barium hexaferrites. Materials Research Bulletin, 145, 558–564.

[27] Shifa, M. S., Khan, W. A., Al-balawi, H., Al-Muhimeed, T. I., Al-Obaid, A. A., Mahmood, Q., & Qureshi, I. (2021). Effects of heat treatment on the structural, spectral, morphological, dielectric, and magnetic properties of Ba0.5Sr0.1Zn0.4Fe12O19 barium ferrites. Ceramics International, 47(8), 233–239.

[28] Gordani, G. R., Ghasemi, A., & Saidi, A. (2003). Enhanced magnetic properties of substituted Sr-hexaferrite nanoparticles synthesized by co-precipitation method. Ceramics International, 40(3), 4945–4952.

[29] Ghasemi, A., Hossienpour, A., Morisako, A., Liu, X., & Ashrafizadeh, A. (2008). Investigation of the microwave absorptive behavior of doped barium ferrites. Materials & Design, 29(1), 112–117.

[30] Lee, J. H., & Kim, Y. J. (2008). Photoluminescent properties of Sr2SiO2:Eu2+ phosphors prepared by solid-state reaction method. Materials Science and Engineering: B, 146(1–3), 99–102.

[31] Smith, J. B., & Norby, T. (2006). Cation self-diffusion in LaFeO3 measured by the solid-state reaction method. Solid State Ionics, 177(7–8), 639–646.

[32] Hessien, M. M., & Rashad, M. (2009). Synthesis and magnetic properties of strontium hexaferrite from celestite ore. Journal of Alloys and Compounds, 476(1–2), 373–378.

[33] Ebrahimi, S. S., Kianvash, A., Ponton, C. B., & Harris, I. R. (2000). The effect of hydrogen on composition, microstructure and magnetic properties of strontium hexaferrite. Ceramics International, 26(4), 379–381.

[34] Vander Voort, G. F., Lampman, S. R., Sanders, B. R., Anton, G. J., Polakowski, C., Kinson, & Scott Jr., W. W. (2004). ASM Handbook: Metallography and microstructures (Vol. 9). ASM International.

[35] Pant, P., Bhuvaneswari, S., & Ghosh, N. N. (2008). Chemical methodologies for preparation of micron and nanometer scale ferrites – a mini review of patents. Recent Patents on Nanotechnology, 2(1), 8–18.

[36] Kokalj, A. (2003). Computer graphics and graphical user interfaces as tools in simulations of matter at the atomic scale. Computational Materials Science, 28(2), 155–168.

[37] Zak, A. K., Majid, W. H. A., Abrishami, M. E., & Yousefi, R. (2011). X-ray analysis of ZnO nanoparticles by Williamson–Hall and size–strain plot methods. Solid State Sciences, 13(1), 251–256.

[38] Goldstein, J. I., Newbury, D. E., Michael, J. R., Ritchie, N. W. M., Scott, J. H. J., & Joy, D. C. (2018). Scanning electron microscopy and X-ray microanalysis (4th ed.). Springer.

[39] Chauhan, P., & Sharma, P. (2010). Magnetic properties of barium ferrites prepared by hydrothermal synthesis. Key Engineering Materials, 655(3), 111–121.

[40] Foner, S. (1959). Versatile and sensitive vibrating-sample magnetometer. Review of Scientific Instruments, 30(7), 548–557.